Numerical Study of Large-Scale Control in Compressible Turbulent Channel Flows

Moghees Ahmad, M. F. Baig, and S. F. Anwer

Abstract Direct numerical simulations in a fully developed compressible turbulent channel flows have been carried out using the large-scale control of large vortical structures along streamwise direction. Effectiveness of the control at Mach number, $Ma = 1.5$ and Reynolds number $Re_b = 3000$ is studied for different amplitudes and wavelengths of forcing. The large-scale control concentrates the turbulent kinetic energy in certain regions near the walls and it can be observed in $y - z$ plane of the channel. These high turbulent kinetic energy regions are also the regions of high streamwise vorticity as well. The control reduces the wall-normal velocity fluctuations near the walls for all the cases but, on the other hand, Reynolds shear stresses are reduced for drag reduction cases and are increased for the case where drag increases. The skin-friction drag reduction(DR) of around 7% is achieved in the present study while, for the case with high strength vortical structures, the skin-friction drag increases.

1 Introduction

The turbulence is an inescapable phenomenon in fluid dynamics and to be precise in our daily life as well. The manipulation of turbulent flows to achieve skin-friction drag reduction is desired, to achieve the benefits related to environmental and economic concerns. Various methods and controls are proposed to achieve this target of taming turbulence. The control methods to contain turbulence are characterized into passive and active control methods based on their input. Passive control techniques require no power input, while active control methods require continuous power input for

M. Ahmad (✉) · M. F. Baig · S. F. Anwer
Department of Mechanical Engineering, Aligarh Muslim University, Aligarh 202002, India
e-mail: mahmad37@myamu.ac.in

M. F. Baig
e-mail: mfbaig.me@amu.ac.in

S. F. Anwer
e-mail: sfahadanwer@zhcet.ac.in

M. A. Siddiqui et al. (eds.), *Advances in Heat Transfer and Fluid Dynamics*, Lecture Notes in Mechanical Engineering, https://doi.org/10.1007/978-981-99-7213-5_2

maintaining the desired changes in the flow. Passive methods such as riblets, coatings, splitter plate, etc., are rather easy but give limited drag reduction of up to 10%. Considerable research has been performed on passive devices like compliant surfaces, wavy walls and riblets [1].

Schoppa and Hussain [2] proposed a new method to control the drag which they named large-scale control. In this control strategy, large-scale vortices are generated along the flow in the streamwise direction. These large-scale vortices affect the near-wall coherent structures responsible for turbulence generation; by mitigating wall-normal vorticity and streaks formation. Schoppa reported 20% drag for certain wavelengths and strengths of the vortices. Canton et al. [3] further investigated the large-scale control by carrying out DNS study at different friction Reynolds numbers (Re_τ) of 104 and 180 and for five different wavelengths. Canton et al. [3] found that the control strategy by Schoppa and Hussain [2] is only provisionally effective and hence suggested a modification to sustain drag reduction and reported drag reduction of around 18%.

This paper aims to study large-scale control in compressible turbulent flows in order to see the efficacy of the control for supersonic flows and to analyse related physics, as this problem has not been explored yet. The results can be applied to transport of compressible gases in rectangular/circular duct flows.

2 Numerical Setup

The dimensional governing equations used for compressible channel flows are listed:

$$\frac{\partial \rho}{\partial t} + \frac{\partial (\rho u_i)}{\partial x_i} = 0 \tag{1}$$

$$\frac{\partial (\rho u_i)}{\partial t} + \frac{\partial (\rho u_i u_j)}{\partial x_j} = -\frac{\partial p}{\partial x_i} + \frac{\partial \tau_{ij}}{\partial x_j} + \rho f_i \tag{2}$$

$$\frac{\partial (\rho e)}{\partial t} + \frac{\partial (\rho e + p) u_i}{\partial x_i} = \frac{\partial (\tau_{ij} u_j)}{\partial x_i} + \rho f_i u_i + \frac{\partial (q_i)}{\partial x_i} \tag{3}$$

where ρ is the density of fluid, t is the time, u_i is the velocity component along x_i direction, e is the total specific energy of the fluid, p is the pressure in the flow field, τ_{ij} is stress tensor and f_i is the driving force.

The present numerical study is performed with an in-house, finite difference code developed for compressible turbulent channel flows and parallelized in all three directions using Message Passing Interface(MPI). A hybrid scheme is used for discretization of the convective or non-linear terms of the governing equations, in which third-order upwinding [4] or fourth-order central differencing is used. Cell-based Peclet number (Pe), $Pe = \rho u_i \Delta x_i / \mu$ is the parameter which decides the discretization of

the convective terms, where Δx_i is the step size of the computational domain and u_i is the velocity of the ith direction. For streamwise and spanwise directions, if the $|\ Pe\ | < 2$, fourth-order central differencing is used and for $|\ Pe\ | \geq 2$, upwinding is used. While, for the wall-normal direction, Peclet number value which decides between upwinding and central differencing is $Pe = 0.2$, if $|\ Pe\ | \geq 0.2$ then upwinding is used otherwise central differencing is used. The cell Peclet number-based discretization had been studied and tested by previous studies as well [5–8]. The diffusive and pressure terms are discretized using fourth-order central difference discretization. The temporal integration is done using second-order Runge–Kutta method due to its efficiency and accuracy.

The directions x, y and z are along streamwise, spanwise and wall-normal, respectively. The channel length $\mathsf{L_x}$, $\mathsf{L_y}$ and $\mathsf{L_z}$ in the x, y and z directions are $4\pi\delta \times 4\pi\delta/3 \times 2\delta$, where δ is the half-channel height. The flow through channel is periodic in spanwise and streamwise directions, respectively, while no-slip condition is applied on the channel walls. The mesh is uniform in streamwise and spanwise directions, while non-uniform mesh is used in the wall-normal direction to capture the small-scale structures close to the channel wall. The number of mesh points considered for x, y and z directions are $192 \times 130 \times 160$, respectively. The bulk Reynolds number is taken $Re_b = 3000$ at Mach number, $Ma = 1.5$ for the present study. The grid spacing for x and y directions in viscous scale is $\Delta x^+ \approx 14$ and $\Delta y^+ \approx 7$, while, for wall-normal direction 'z', it varies from $\Delta z^+_{min} \approx 0.04$ to $\Delta z^+_{max} \approx 4.2$. The resolution in wall-normal direction is finer than that of Kolmogorov scale, which is 0.53 in viscous scale. Two-point correlations both in streamwise and spanwise directions confirm that the dimensions of the channel are sufficient for the computations. The code is validated with results from Coleman et al. (CKM) [9].

The large-scale vortices are produced by using the body force method as proposed by Canton et al. [3]. The dimensional equations for the body forces are

$$f_{x_{con}} = 0 \tag{4}$$

$$f_{y_{con}}(y, z) = -A\beta\ cos(\beta y)(1 + \ cos(\pi(\frac{z}{h} - 1))) \tag{5}$$

$$f_{z_{con}}(y, z) = -A\pi\ sin(\beta y)\ sin(\pi(\frac{z}{h} - 1)) \tag{6}$$

where $f_{x_{con}}$, $f_{y_{con}}$ and $f_{z_{con}}$ are the control on the body forces in x, y and z directions, respectively. A is the amplitude of the force applied for the generation vortices and β is the wavenumber of the spanwise length of the vortices.

3 Results and Discussion

With the aim to gain insight into the large-scale control and to study the changes it brings to the physics of the flow, a number of numerical simulations are carried out by varying forcing amplitude and spanwise wavelength of the vortices for compressible turbulent channel flows. The wavelength of the vortices is denoted by $\Lambda^+ = 2\pi\beta^+$. The control is applied to a fully developed compressible turbulent channel flow field at $Re_b = 3000$ and $Ma = 1.5$. The Dirichlet boundary condition is used on the turbulent channel walls. Table 1 shows the parametric details of the simulations performed. The wavelength $\Lambda^+ = 900$ is selected for the simulations and one case of $\Lambda^+ = 450$ is also simulated, where $\Lambda^+ = 900$ corresponds to one pair of vortices, while $\Lambda^+ = 450$ corresponds to two pairs of vortices in the $y - z$ plane. The strength of the vortices produced is determined by quantity $\max|\langle w\rangle_{(y,z)}|$ which is the maximum value of wall-normal velocity component in $y - z$ plane obtained by averaging in streamwise direction x and time t. The skin-friction drag reduction DR is calculated by the mathematical equation Eq. (7).

$$DR\% = \frac{\tau_w|_{unc} - \tau_w|_{con}}{\tau_w|_{unc}} \times 100 \tag{7}$$

where subscript 'unc' refers to uncontrolled case and 'con' to controlled case.

The control is applied throughout the axial length of the channel and to quantify the effect of the control, the temporal variation of the wall shear stress is recorded. The averaging of the variables is done in streamwise direction x and time t, hence depicted in $y - z$ plane and the averaged quantity is denoted by $\langle * \rangle_{y,z}$. Figure 1 shows contour plots of vortices produced by large-scale control in $y - z$ plane of the channel. Here, Fig. 1a shows two pairs of vortices produced for Case 3 and Fig. 1b shows one pair of vortices produced for case 4. These plots show the cross-flow velocity with velocity vectors superimposed onto the contours of cross-flow velocity to show the rotation of the vortices. It can be observed from Fig. 1b that the large-scale control aggregates the streaks at the bottom wall from where the fluid lifts up from the bottom to top wall and on outer sides at the top wall. Mean streamwise vorticity $\overline{\omega}_x$ are shown in $y - z$ plane, Fig. 2. These plots show the high vorticity concentration areas in the $y - z$ plane. The mean streamwise vorticity $\overline{\omega}_x$ has high values in regions where the fluid lifts up and settles or spreads out onto the wall due

Table 1 Simulations details

Case	Ma	Re_b	A	Λ^+	$\max\|\langle w\rangle_{(y,z)}\|$	$DR\%$
1	1.5	3000	0.00025	900	3.3	2.92
2	1.5	3000	0.0005	900	11.03	2.89
3	1.5	3000	0.0005	450	7.7	7.2
4	1.5	3000	0.00075	900	13.8	−4.5

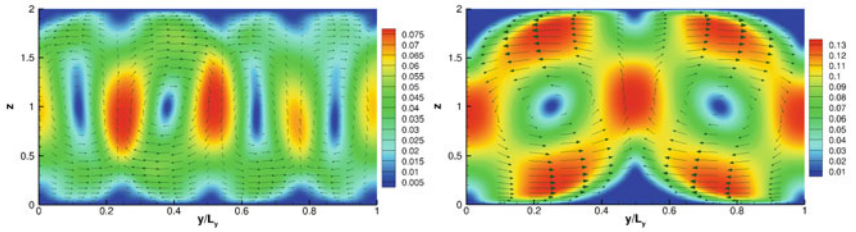

Fig. 1 Cross-flow velocity plots averaged in x & t for $y-z$ plane **a** Case 3, **b** Case 4

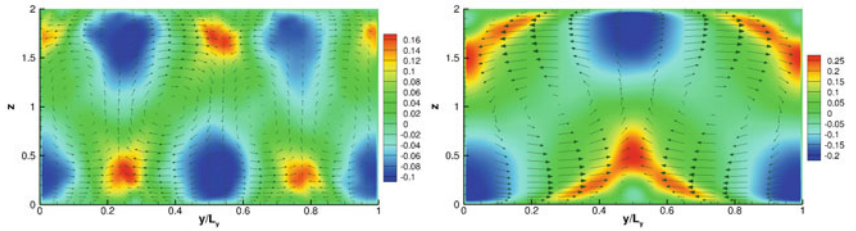

Fig. 2 Mean streamwise vorticity $\overline{\omega}_x$ plots averaged in x & t for $y-z$ plane **a** Case 3, **b** Case 4

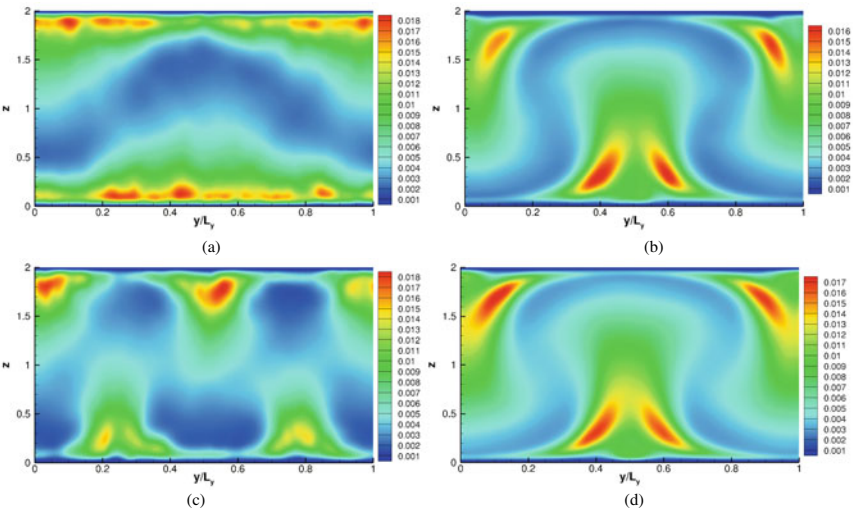

Fig. 3 Comparison of Turbulent kinetic energy (TKE) in y-z plane **a** Case 1, **b** Case 2, **a** Case 3, **b** Case 4

to high shear rate. As can be seen from $\overline{\omega}_x$ contour plots, that for drag reduction case, i.e. case 3, the values of $\overline{\omega}_x$ are less than that for drag increase case, i.e. case 4.

Figure 3 depicts the turbulent kinetic energy (TKE) distribution across the channel in $y - z$ plane. The turbulent kinetic energy is concentrated in the regions where the fluid lifts up from the wall. Figure 3a shows regions of low and high TKE for case 1 which has low forcing amplitude. It can be observed that regions of high TKE are spread in lift-up fluid regions near the wall, whereas low TKE regions are loosely spread across the channel as compared to other cases. Figure 3c shows pattern of high and low TKE regions for two pairs of vortices, while cases 2 & 4 have one pair of strong vortices and show similar plots as in Fig. 3b, d. However, the intensity of high TKE regions is considerably more for drag increase (DI) case, i.e. case 4. The spread of low TKE regions in cases 2 & 4 leads to horseshoe pattern.

Statistical plots for the bottom half of the channel are shown in Fig. 4 as they help visualize mean variation in wall-normal direction. These have been obtained after planar averaging in $x - y$ plane followed by time averaging. The RMS values of streamwise velocity component u', wall-normal component w' and Reynolds shear stresses $\overline{\rho u' w'}$ of the controlled cases are compared with the uncontrolled case. To magnify the near-wall variation of these plots log-scale is used for wall-normal distance. Figure 4a compares the RMS plots of streamwise velocity component u' of all the controlled cases along with the uncontrolled case for bottom half of the turbulent channel. Case 1 has the lowest forcing amplitude and hence its effect on the flow is minimal. For cases 1 & 3, u' is less than that of the uncontrolled flow in the near-wall region which signifies reduction in skin-friction drag, whereas, for Cases 2 & 4, the quantity u' has increased as compared to uncontrolled case. The case with drag increase, i.e. case 4 has the highest u' plot throughout the channel, which leads to an increase in skin-friction drag. The RMS values of wall-normal velocity component w' are an important quantity for turbulence control and they are depicted in Fig. 4b. For all cases pertaining to drag reduction as well as drag increase, there is a drop in w' in near-wall region of the turbulent channel flow. However, for the drag increase case, w' increases to a very high value as the curve approaches the centre of the turbulent channel. This increase in w' at the centre of the channel is attributed to high forcing amplitude which in turn increases the quantity $\max|\langle w \rangle_{(y,z)}|$ as well. The Reynolds shear stresses ($\overline{\rho u' w'}$) averaged in wall-normal direction are shown in Fig. 4c. As can be seen from the plot, Reynolds shear stresses have decreased for the cases where drag has reduced and also their peak has shifted away from the wall. Case 1 has little variation from uncontrolled case as low forcing amplitude hardly affects the channel statistics. For all the controlled cases except Case 4, $\overline{\rho u' w'}$ has reduced and also shifted away from the wall as well. However, for Case 4, $\overline{\rho u' w'}$ has increased in magnitude and its peak has also moved closer to the wall as compared to the uncontrolled case, signifying an increase in the skin-friction drag.

The vortical structures which signify the intensity of the turbulence are shown in Fig. 5 for all the cases studied, along with the vortical structures for uncontrolled turbulent channel flow. The Q-criterion which was proposed by Hunt [10] is used to visualize the iso-surfaces of the vortical structures. The streamwise velocity component u is superimposed on these vortical structures as well. The vortical structures for only the bottom half of the channel are shown in these plots. It can be observed from Fig. 5 that, for all the controlled cases, there is concentration of the vortical

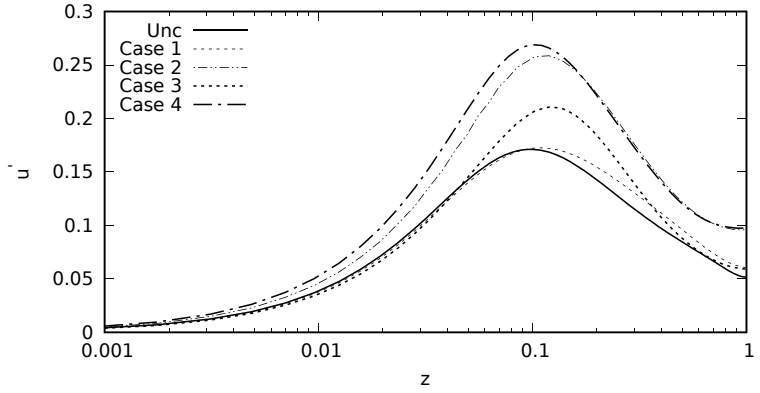

(a)

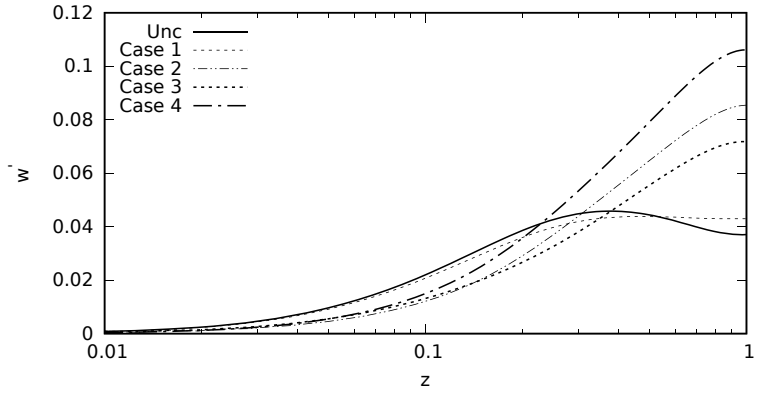

(b)

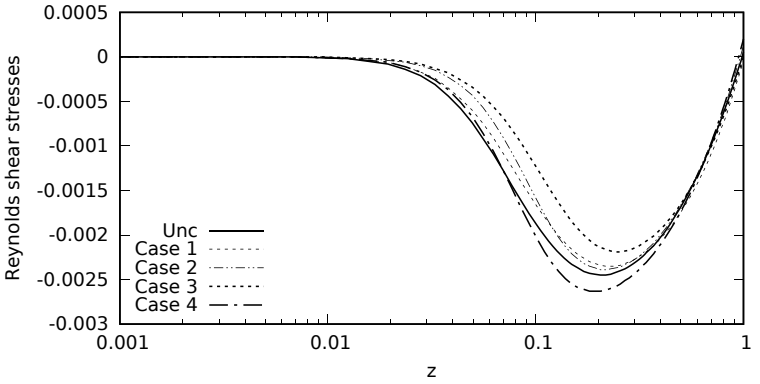

(c)

Fig. 4 Comparison of RMS quantities for uncontrolled and controlled cases averaged in wall-normal direction, bottom half of channel is shown **a** RMS of Streamwise velocity component, u', **b** RMS of Wall-normal velocity component, w', **c** Reynolds shear stresses, $\overline{\rho u' w'}$

structures near the wall surface from where the fluid lifts up from the wall. At the bottom wall, high density of vortical structures occurs at the centre of the channel for Cases 1, 2 & 4 which have one pair of vortices, while, for case 3, high concentration of vortical structures is observed at two locations, as it has two pair of vortices. At

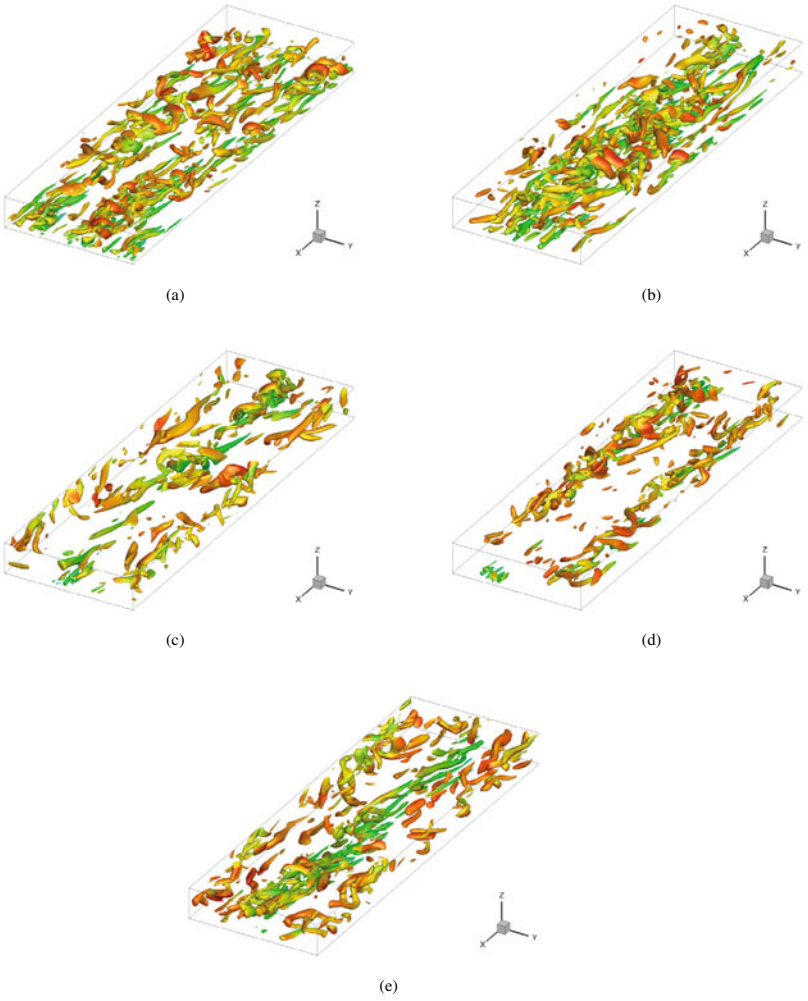

Fig. 5 Iso-surfaces visualization using Q-invariant criterion at a value of Q=0.28, **a** Uncontrolled case, **b** Case 1, **c** Case 2, **d** Case 3, **e** Case 4

the top wall of the channel, these structures are found near the outer sides of the wall. For high-strength cases, the small-scale vortical structures are being moved in a circulatory fashion by the large-scale vortical structures.

4 Conclusions

Numerical simulations of a fully developed compressible turbulent channel flow have been carried out by generating large-scale vortical structures along the streamwise direction. The effectiveness of the control for Mach number, $Ma = 1.5$ and Reynolds number $Re_b = 3000$ is studied at different amplitudes of forcing and wavelength. The large-scale control leads to concentration of vortical structures on the bottom and top walls, leading to zones of high and low turbulent kinetic energy. In the near-wall region, the control decreases the wall-normal velocity fluctuations monotonically; however, Reynolds shear stresses decrease for drag reduction cases and increases for drag increase cases. The drag reduction of $\approx 7\%$ is achieved in the present study, while, for high forcing amplitude of the large-scale vortices, the drag increases in the channel flow.

References

1. Gad-El-Hak M (2000) Flow control
2. Schoppa W, Hussain F (1998) A large-scale control strategy for drag reduction in turbulent boundary layers. Phys Fluids 10:1049–1051. https://doi.org/10.1063/1.869789
3. Canton J, Örlü R, Chin C, Hutchins N, Monty J, Schlatter P (2016) On large-scale friction control in turbulent wall flow in low Reynolds number channels. Flow Turbul Combust 97:811–827
4. Veersteg H, Malalasekera W (1995) An introduction to computational fluid dynamics
5. Ahmad H, Baig MF, Fuaad PA (2015) Numerical investigation of turbulent-drag reduction induced by active control of streamwise travelling waves of wall-normal velocity. Eur J Mech B Fluids 49:250–263. https://doi.org/10.1016/j.euromechflu.2014.09.004
6. Fuaad PA, Baig MF, Ahmad H (2016) Drag-reduction in buoyant and neutrally-buoyant turbulent flows over super-hydrophobic surfaces in transverse orientation. Int J Heat Mass Transfer 93:1020–1033. https://doi.org/10.1016/j.ijheatmasstransfer.2015.10.068
7. Khawar O, Baig MF, Sanghi S (2021) Taylor-couette flows undergoing orthogonal rotation subject to thermal stratification. Phys Fluids 33:035107. https://doi.org/10.1063/5.0035546
8. Naim MS, Baig MF (2019) Turbulent drag reduction in taylor-couette flows using different super-hydrophobic surface configurations. Phys Fluids 31:095108. https://doi.org/10.1063/1.5116316
9. Coleman GN, Kim J, Moser RD (1995) A numerical study of turbulent supersonic isothermal-wall channel flow. J Fluid Mech 305:159–183. https://doi.org/10.1017/S0022112095004587
10. Hunt JCR, Wray AA, Moin P (1988) Eddies, streams, and convergence zones in turbulent flows. Publisher Centre for Turbulence Research